Observations of upper ocean boundary layer dynamics in the marginal ice zone

Ilker Fer[1,2] and Arild Sundfjord[2,3,4]

[1]   Vertical profiles of turbulent kinetic energy dissipation and small-scale hydrography were collected in the upper ocean boundary of both ice-covered and ice-free stations in the marginal ice zone of the Barents Sea in spring 2005. Together with shipboard wind measurements and current profiles, the mixed and mixing layer dynamics are studied. During the survey, shear production by the stress at the surface or under the ice dominated. Large upward turbulent heat fluxes $\sim$300–500 W m^{-2} were calculated for the mixing layers overlying the warm Atlantic Water which compared well with those obtained from an independent parameterization. At the top of the pycnocline, corresponding heat fluxes were 10–20 W m^{-2}. Significant stabilizing buoyancy fluxes were estimated for ice-drift stations owing to the melting of ice in response to the large heat fluxes. The mean dissipation profile in the ice-free reference station agreed with the constant-stress wall layer scaling within 30%. On the contrary, the observed dissipation profiles were enhanced in the upper half of under-ice mixing layer or within 2.5 times the assessed pressure-ridge keel depth. Deeper in the mixing layer the profiles relaxed toward the wall scaling. The variability of dissipation in the mixed layer was better captured by the shear production profile when local friction speed was used together with a mixing length profile modified by buoyancy fluxes. Significant correlations were found between dissipation integrated over the mixing layer and work done by stress under the ice and the wind work at 10 m height. The low correlation between the mixed layer depth and length scale for neutral conditions significantly increased when the reduction in the mixing length due to buoyancy fluxes was accounted for. The mixing depth is observed to be strongly correlated with the outer neutral planetary length scale.

1.   Introduction

[2]   Among the ice-covered Polar regions, the marginal ice zones (MIZ) where ice concentration ranges from open water to consolidated pack ice are the most physically and biogeochemically active areas. Relying on the present understanding of the air-sea-ice interaction and its parameterization, *Smith and Niebauer* [1993] conclude that the ice-edge phytoplankton bloom cycle is primarily regulated by vertical stratification whereas the spatial extent of the bloom is controlled by the ice dynamics and the response to wind forcing. Vertical mixing in the MIZ and the dynamics of the surface and under-ice mixed layer will therefore have direct influence on the food web and carbon cycle.

[3]   The Barents Sea is a key region for water mass modification [*Pfirman et al.*, 1994]. This is manifested by the observation that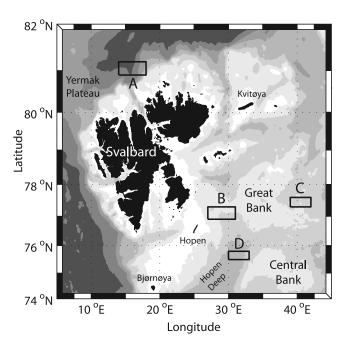 while a majority of the inflow to the Barents Sea from a transect between north of Norway and Bjørnøya is Atlantic Water (AW, hereinafter) with temperature > 3 °C [*Ingvaldsen et al.*, 2004], only 25% of the Barents Sea water that enters the Arctic Ocean through a section between Novaya Zemlya and Franz Joseph Land (the main exit to the Artic Ocean) has temperature > 0 °C [*Schauer et al.*, 2002]. The MIZ in the Barents Sea is a frontal zone caused by the interaction of cold-fresh melt-water and this relatively warm and salty modified water of Atlantic origin. The MIZ here is characterized by significant biological production [*Falk-Petersen et al.*, 2000] and large biomass compared with the interior Arctic Ocean [*Sakshaug*, 2004]. In addition to the enhanced biological carbon cycling, inorganic carbon fluxes can also be large, owing to increased ability to dissolve and absorb CO_2 of the cooled through-flowing AW [*Kaltin et al.*, 2002].

[4]   It is the purpose of this paper to report on observations of turbulence in the near-surface and under-ice mixed layer of the MIZ in the Barents Sea, during early melting conditions. The data set presented herein was collected from the R/V *Jan Mayen* during the last of a series of multidisciplinary cruises of the "Carbon flux and ecosystem feed back in the northern Barents Sea in an era of climate

---

[1]Bjerknes Centre for Climate Research, Bergen, Norway.
[2]Geophysical Institute, University of Bergen, Bergen, Norway.
[3]Norwegian Polar Institute, Tromsø, Norway.
[4]Now at Norwegian Institute for Water Research, Tromsø, Norway.

Figure 1. Location map of the study site with place names and occupied stations (A, B, C, and D) indicated by boxes covering the approximate spatial extent of each drift. The isobaths are 100, 200, 300, 500, 1000, and 2000 m.

change" (CABANERA) project as a joint effort of the CABANERA and the Polar Ocean Climate Processes (ProCLIM) projects. A more detailed description of the hydrography, fine-scale, and turbulence characteristics comprising the surveys of both 2004 and 2005 is reported by *Sundfjord et al.* [2007]. In the next section we give a brief description of the measurements and survey. In section 3 we summarize the observations of the environmental forcing and upper mixed layer dynamics, and subsequently in section 4 we present and discuss our results. We examine the vertical structure of the dissipation of turbulent kinetic energy, ε, with respect to constant-stress scaling (section 4.1), a local stress scaling incorporating the effect of stabilizing buoyancy flux (section 4.4), and a modified version of the law of the wall (section 4.5). In section 4.2, we attempt to delineate the influence of pressure ridge keels which might impose considerable drag. Heat flux and vertical eddy diffusivity in the upper ocean boundary (section 4.3), integrated dissipation in the mixed layer (section 4.6) and the dependence of the observed mixed and mixing layer depths to the wind stress forcing and related parameters (section 4.7) are discussed.

[5] In this study, we employ a right-handed coordinate system with the vertical positive upward. The day of the year is given with the convention that day 0.5 is 1200 UTC on 1 January 2005. Salinity is calculated using the practical salinity scale. In order to facilitate reading we name the stations A−D (section 2), which corresponds to stations XIV, XVI, XVII, and XVIII, respectively, of the cruise log and of *Sundfjord et al.* [2007].

2. Measurements

[6] Measurements of hydrography, fine-scale current profiles and temperature/shear microstructure were made dur-

ing 18 May to 4 June 2005 in the MIZ around the Svalbard Archipelago. The survey covered ice stations drifting north of Svalbard at ∼2000-m depth (Station A) in the northern part of Hopen Deep (Station B) and near the Great Bank (Station C). A reference station was occupied in ice-free water (Station D) in Hopen Deep close to the Central Bank. The stations are shown in Figure 1 and summarized in Table 1 (for a detailed description, see *Sundfjord et al.* [2007]).
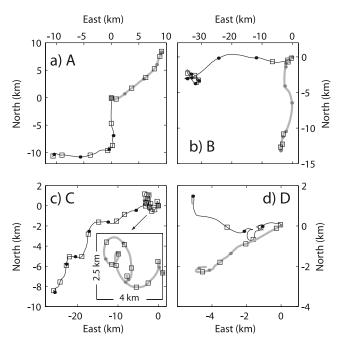
[7] At stations, continuous current profiles were collected and averaged every 5 min from the vessel-mounted 150-kHz RD-Instruments ADCP at 4-m bins from 15 m to a last good bin at ∼ 250 m. Ship velocity derived from navigation is representative of the ice velocity for drift stations. Wind speed and direction were acquired by the ship weather station every minute whereas the temperature sensor malfunctioned. Ice cover percentage was assessed subjectively from the vessel. Ice draft and pressure ridge keel depths were measured by divers using pressure gauges along multiple transects below the large main ice floe near which all the sampling was done. The ice parameters given in Table 1 are representative of the stations although we cannot assess the degree of local variability.

[8] The microstructure data were collected at 1024 Hz using a loosely tethered free fall MSS profiler [*Prandke and Stips*, 1998] equipped with airfoil shear probes and fast response conductivity and temperature (FP07) sensors. The profiler comprises an acceleration sensor and conventional CTD sensors for precision measurements. Microstructure data are processed as described by *Fer* [2006]. The dissipation rate of turbulent kinetic energy per unit mass, ε in units W kg^{-1}, is calculated using the isotropic relation $\varepsilon = 7.5\nu \langle u_z^2 \rangle$, where ν is the viscosity of seawater (within 1.6− 1.9×10^{-6} m^2 s^{-1} for the recorded range of temperatures −1.8 to 5 °C), u_z is the shear of the horizontal small-scale velocity, and angle brackets denote appropriate averaging. The instrument fall speed (0.7−0.8 m s^{-1}) is used to convert from frequency domain to vertical wavenumber domain using Taylor's hypothesis, and the shear variance is obtained by iteratively integrating the reliably resolved portion of the shear wavenumber spectrum of half-overlapping 1-s segments. Narrowband noise peaks induced by the probe guard cage are above the wavenumber

Table 1. Summary of Occupied Stations[a]

	Station A	Station B	Station C	Station D
Latitude, start, °N	81° 07.6′	77° 08.4′	77° 25.7′	75° 40.5′
Longitude, start, °E	16° 19.0′	29° 56.7′	41° 02.8′	31° 47.8′
Start time, DOY	139.2	144.2	147.0	149.9
Duration, hours	26.7	43.3	36.9	44.5
Bottom depth, m	2000	200	220	340
Ice cover, I, %	50	80−90	60−70	0
Ice thickness, h_i, m	1.0	0.9−1.1	3.0−3.2	0
Keel depth, h_{keel}, m	4.8−6.3	4.7	3.7−4.0	0
u_{*0}, m s^{-1}	0.023	0.017	0.015	0.02
θ, °C	−0.80	−1.31	−1.76	3.12
S	34.20	34.19	34.31	35.09
MSS sets	7	5	11	5
Total MSS profiles	21	13	32	15

[a]Time is given as day of year (DOY) in 2005 with 1200 UTC on 1 January equal to 0.5. Duration is the time between the first and last microstructure profiler (MSS) cast for each station. Bottom depth recorded by the ship echo sounder and estimated friction speed are averaged over the duration of the station. Potential temperature and salinity are averages over the mixed layer depth over the ensemble of MSS sets.

Figure 2. (a–d) Progressive vector diagrams derived from 12-hour smoothed ship velocity (black lines, representative of the ice drift in Figure 2a–2c) and depth-averaged current (thick gray lines). Solid circles are placed at 6-hour intervals; the solid squares are placed at the mean time of each microstructure profiler (MSS) set. The diagrams cover the durations identified in Figure 3, except that Figure 2d terminates ∼24 hours before the last MSS set. The depth-averaged current in Figure 2c is enlarged in a box of 4 km × 2.5 km to show the near-inertial period loops.

range chosen for the analysis. Typical commonly accepted uncertainty in ε measurements is a factor of two [*Moum et al.*, 1995]. Dissipation data in the upper 5–8 m are unreliable owing to contamination of the ship's wake as well as the initial adjustment to the free fall. The profiles of precision CTD (corrected against available SeaBird CTD profiles) and ε are produced as 10-cm and 50-cm vertical averages, respectively. Typically, a sequence of three microstructure profiles (set hereafter) was acquired every 3–6 hours over typical station duration of 26–45 hours (Table 1). The collection of each set typically lasted 0.5–1 hours. A set ensemble of 50-cm vertical-bin-averaged dissipation profiles thus consists of six data points when both shear probes acquired acceptable data.
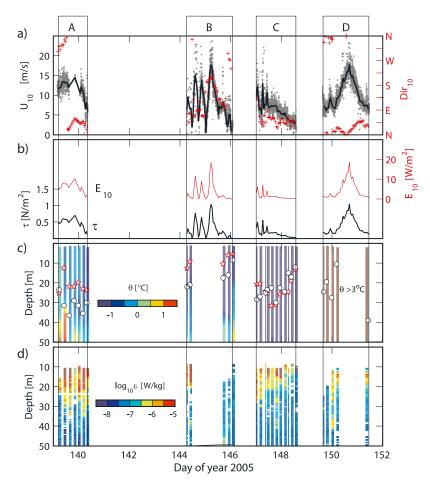
3. Observations

[9] Station A, north of Svalbard, is located where the continental slope branch of warm and relatively salty AW transported by the West Spitsbergen Current enters the Arctic. The West Spitsbergen Current is observed to split into multiple branches in the Fram Strait [*Quadfasel et al.*, 1987], and the part that flows along the Svalbard continental slope and crosses the Yermak Plateau is possibly the strongest [*Bourke et al.*, 1988]. The reader is also referred to relevant papers of dedicated surveys on turbulent mixing during an ice drift in the Yermak Plateau where measurements revealed upward oceanic heat fluxes reaching 30 W m^{-2}

owing to energetic mixing events as a result of proximity to internal wave sources [*Padman and Dillon*, 1991; *Wijesekera et al.*, 1993].

[10] Over the duration of drift A, initially southward and then westward, the depth-averaged currents were toward northeast (Figure 2a). The average temperature of $\theta = -0.8$ °C in the under-ice mixed layer was significantly above the freezing point for the observed salinity at atmospheric pressure T_f (S = 34.2, P = 0) of -1.88 °C. This is owing to the upward vertical heat flux from the underlying warm AW (quantified later in section 4.3). For similar mixed layer values of S, the average θ in the interior Barents Sea was significantly lower, emphasizing the strong heat loss AW encounters en route through the shallow Barents Sea (section 1). Particularly toward the east of the Great Bank, the temperature in the under-ice mixed layer was close to the freezing point with negligible warming, hence contribution to melting, from AW.

[11] The along-track observations of wind forcing together with upper 50-m potential temperature, θ, and dissipation, ε, are shown as a time series in Figure 3. The instantaneous wind speed (Figure 3a, shaded crosses) reached strong gale scale (20.8–24.4 m s^{-1}) both during stations B and D, forcing interruption of MSS sampling. Both the magnitude and direction of wind velocity at B were highly variable. The energy flux at 10 m height, $E_{10} = \tau U_{10}$ where τ is the wind stress and U_{10} is the wind speed at 10 m, was largest at A (6.3 ± 2.3 W m^{-2}) and lowest at C (1.2 ± 1.5 W m^{-2}) when averaged (± one standard deviation) over the duration of the station. The wind stress, $\tau = \rho_a C_D U_{10}^2$, is calculated using air density $\rho_a = 1.25$ kg m^{-3} and drag coefficient $C_D = 2.7 \times 10^{-3}$ (section 4.1). The influence of the large energy flux at B is clearly seen on the ship (ice drift) and depth-averaged water velocity progressive vector diagrams (Figure 2b). During relatively calm C, the wind direction was also stable (Figure 3a) and the ice drift was at ∼20° to the right of the northeasterly wind. The nearly stationary semidiurnal loops of the depth-averaged current at C (Figure 2c) indicate very little net transport during the ice station time. At open water station D the vessel followed a set of drifting sediment traps, so that the vessel drift was representative of the mean water current of the upper ∼50 m and not the true surface current speed.

[12] The surface mixed layer is often defined as the upper layer of the ocean with quasi-homogeneous potential density above the pycnocline. Its thickness, referred to as mixed layer depth D_{mixed}, is most commonly determined by various threshold methods as the depth where a property (e.g., density, temperature, or their vertical gradients) first exceeds a prescribed threshold. Resulting estimates of D_{mixed} are often sensitive to the choice of method and thresholds and sometimes do not agree with what the "eye" would pick, and require manual corrections. Relative performance of various methods was reported by *Thomson and Fine* [2003] who also proposed a split-and-merge method to determine D_{mixed}. In this study we adopt an improved version of the split-and-merge method (R. Thomson, personal communication, 2005), which includes an additional run of the split-and-merge procedure using a lower boundary depth determined by the first run. The sensitivity of the result to the initial choice of parameters is greatly reduced. In our data set, credible mixed layer depths for
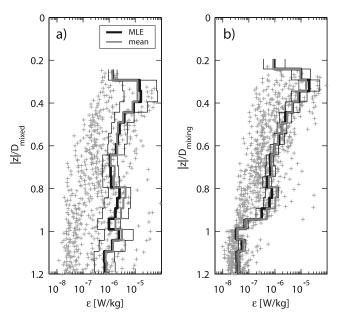
Figure 3. Overview of along-track (a) wind speed, U_{10}, and direction, (b) wind stress, τ, and work, E_{10}, MSS-derived set-averaged color-coded profile of (c) potential temperature, θ, and (d) dissipation, ε. Wind data are recorded at $\sim$10 m from the ship weather station. The 1-min wind velocity record (speed shown as gray crosses in Figure 3a) are hourly vector-averaged (black line in Figure 3a), interpolated for missing data prior to calculation of direction, stress, and wind work. Time series cover varying geographic locations (Figure 1). The duration of occupation of the stations is bounded by vertical lines with stations' names indicated at top. Station D is in open water with temperature >3 °C in the upper 50 m. In Figure 3c, open circles are the mixing layer depth, whereas red stars are the mixed layer depth. The typical duration of each MSS set is about 1 hour; however, the width of the color-coded columns in Figure 3c and 3d are arbitrary, $\sim$3 hours, for clarity.

different hydrographic conditions were more consistently identified compared to those derived from threshold criteria. The occupied drift stations (A, B, and C) were 50–90% ice covered and the surface mixed layer was in contact with the ice cover (also referred to as under-ice mixed layer).

[13] The mixed layer depth, D_{mixed} (stars in Figure 3c), was shallowest at B and varied within 10–35 m for the drift stations of our survey. An anomalous estimate of D_{mixed} for the second set of A is significantly shallower than the nearby occupations owing to a weak vertical salinity gradient (the temperature is well-mixed down to a depth comparable with D_{mixed} values of other sets). We retain the objective estimate of the split-and-merge algorithm. A mixed layer represents a history of the previous mixing events and is not necessarily subject to mixing at the time of measurement. Therefore a distinction is often made between the mixed layer and the mixing layer [*Dewey and Moum*, 1990; *Padman and Dillon*, 1991; *Brainerd and Gregg*,

1995]. It is only when the mixing layer is deeper than the mixed layer that the turbulent motions work against the stratification and a part of the energy input is used to increase the potential energy of the water column. We define the mixing layer depth, D_{mixing}, as the depth when ε first drops below 3×10^{-8} W kg^{-1}, approximately 3–4 times the instrument noise level. D_{mixing} (circles in Figure 3c) is, on average, deeper than D_{mixed}, suggesting entrainment of stratified water into the mixed layer, albeit occasionally a different pattern can be observed: for example, mixed layer deepens during the first half of C when D_{mixing} decreases.

[14] For the ice-drift stations the depth is converted to distance from the ice bottom, z, using the measured ice thickness and scaled by D_{mixed} or D_{mixing}. Observed profiles of dissipation from all 23 set-averaged profiles from the ice-covered stations are shown in Figure 4 with scaled distance from ice. Values of ε range over 4 decades. The arithmetic mean of ε over 0.05 normalized distance bins agree within

Figure 4. Observed dissipation profiles for the ice-covered stations of the survey, where the ordinate is the vertical distance from the ice, $|z|$, scaled (a) by the mixed layer depth, D_{mixed}, and (b) by the mixing layer depth, D_{mixing}. Presented are set-averaged 23 profiles (gray crosses), their arithmetic mean in 0.05 unit normalized distance bins (gray line), and the maximum likelihood estimate (MLE) values (black line). The MLE line agrees with that of the arithmetic mean within 95% confidence intervals.

95% confidence intervals of the maximum likelihood estimate (MLE) from a lognormal distribution, $\varepsilon_{MLE} = \exp(\mu + \sigma^2/2)$, where μ and σ are the expected value and standard deviation of $\ln(\varepsilon)$, respectively [*Baker and Gibson*, 1987]. On the average, dissipation increases with distance from the ice-water interface down to about $|z|/D_{mixing} \sim 0.3$, decreases linearly down to $|z|/D_{mixing} \sim 0.6$, then remains nearly constant at $\sim 6 \times 10^{-7}$ W kg^{-1} down to $|z|/D_{mixing} \sim 0.9$ before dropping sharply near the mixing layer depth.

4. Mixed Layer Dynamics: Results and Discussion

4.1. Stress Scaling

[15] The main forcing mechanisms in a surface or under-ice mixed layer is surface stress and/or buoyancy forcing or a combination of the two. The average under-ice stress, hence the friction speed, can be obtained from the ice force balance [*McPhee*, 1990]. The steady state force balance, ignoring the internal ice stresses' contribution yields

$$\vec{\tau}_a - \vec{\tau}_0 = jh_i\rho_i f(\vec{U}_i - \vec{U}_g), \tag{1}$$

where the tangential air stress on ice is

$$\vec{\tau}_a = \rho_a C_D |\vec{U}_a - \vec{U}_i|(\vec{U}_a - \vec{U}_i) \quad [\text{N m}^{-2}]. \tag{2}$$

Here, subscripts a and i refer to the atmosphere and ice, j is $(-1)^{1/2}$, h_i is the ice thickness, ρ_i is the ice density, f is the

Coriolis parameter, $\vec{U}$ is the horizontal velocity vector in complex notation ($\vec{U} = u + jv$ where u is the east component and v is the north component of the velocity), C_D is the drag coefficient between air and ice and τ_0 is the tangential stress at the ice-water interface. The contribution of internal stresses to the force balance in the MIZ is negligible and equation (1) can be used to get an estimate of the friction speed under the ice $u_{*0} = \sqrt{|\vec{\tau}_0|}$. We computed the friction speed for the duration of each MSS set (23 sets in total in 3 ice-drift stations) using station mean ice thickness, local value of f, $\rho_a = 1.25$ kg m^{-3}, $\rho_i = 917$ kg m^{-3} and $C_D = 2.7 \times 10^{-3}$, representative for 50% ice-covered outer and diffuse MIZ [*Guest et al.*, 1995]. The geostrophic velocity, $\vec{U}_g$, and ice-drift velocity, $\vec{U}_i$, are assumed to be represented by the depth-averaged current from the vessel-mounted ADCP and smoothed ship navigation, respectively. The geostrophic velocity is the current due to the slope of the sea surface that would exist in the absence of the ice. When $\vec{U}_g$ is approximated as the current at the deepest reliable depth bin of the ADCP (in lieu of depth average), friction speed changes within 6%. All the velocity data are vector averaged for the duration ($\sim$1 hour) of each MSS set prior to calculating u_{*0}.

[16] Under melting conditions destabilizing buoyancy flux is not expected owing to increased stratification caused by accumulation of meltwater under the ice. Estimates of heat flux in the mixed layer show significant oceanic heat flux toward the ice (section 4.3). We therefore assume that there was no turbulent production by destabilizing surface buoyancy flux. This is also the case for the open water station D: Lacking shipboard meteorological data to derive the sea-atmosphere heat flux, we rely on NCEP reanalysis at station D. At the NCEP grid point closest to the station, the net heat flux for the duration of D is $\sim$90 W m^{-2}, toward the ocean (or $\sim$75 W m^{-2}, when adjusted for sensible heat fluxes inferred from CTD). The uncertainty may be large, but we have confidence in the direction of the flux given the large net contribution from the radiation fluxes during the boreal summer. Here, the air temperatures close to the water surface, when inferred from the temperature records when MSS and SeaBird CTD sensors were in air, were 1–2 °C, not significantly different from water temperature of $\sim$ 3°C and thus contributing very little to the total heat fluxes. Stabilizing buoyancy flux from melting sea ice, on the other hand, can be comparable to the other terms in the TKE equation, especially in response to localized large upward heat fluxes. This is discussed further in section 4.4.

[17] In the absence of buoyancy flux and vertical transport of turbulent kinetic energy, in a steady, horizontally homogenous flow, shear production balances dissipation. The dissipation rate, ε, then scales with $\varepsilon_s = u_{*0}^3/\lambda$, where λ is the turbulent length scale. Near a boundary, in the constant-stress layer, the relevant length scale is the distance from boundary, $\lambda = \kappa|z|$ [*Tennekes and Lumley*, 1972], which is often called the law of the wall (LOW). For conditions dominated by wind stress in an oceanic mixed layer, *Lombardo and Gregg* [1989] find $\langle\varepsilon/\varepsilon_s\rangle \sim 1.76$ for $0.25 \leq |z|/D_{mixed} \leq 1$, consistent with atmospheric observations. They attribute the factor 1.76 (i.e., deviation from unity) to possible turbulence production by convection. Large discrepancies are expected and observed [*Gargett*, 1989] when strong winds lead to additional turbulent
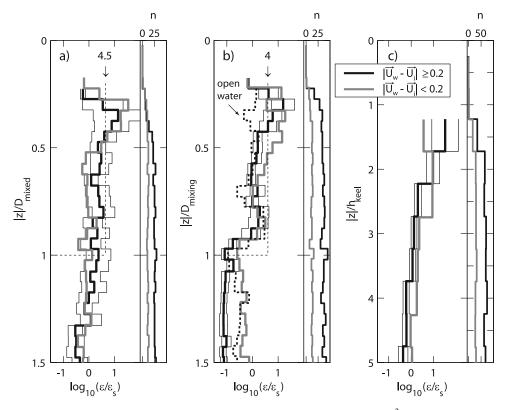
Figure 5. Vertical profiles of dissipation normalized by stress scaling, $\varepsilon_s = u_{*0}^3/\kappa|z|$, where the vertical distance from the ice, $|z|$, is scaled (a) by the mixed layer depth, D_{mixed}, (b) by the mixing layer depth, D_{mixing}, and (c) by the keel height, h_{keel}. The profiles are presented as MLE values over the number of data points, n (shown in narrow adjacent panels), in normalized depth bins (of length equal to 0.05 for Figures 5a and 5b and 0.5 for Figure 5c). The conditions when the magnitude of ice-relative velocity was greater than (black lines) and less than (gray lines) 0.2 m/s are shown separately. The 95% confidence intervals are given for only one profile, for clarity. The average values (over all values of ice relative speed) for the normalized depth ≤ 1 are indicated in Figures 5a and 5b. The dashed line in Figure 5b is the profile derived for the open water station D, shown for reference.

processes, for example, wave-breaking [*Agrawal et al.*, 1992] bubbles, and coherent structures of Langmuir circulation [*Thorpe et al.*, 2003]. In the under-ice boundary layer the influence of pressure ridge keels and irregular under-ice surface roughness and topography can disrupt the flow [*McPhee*, 2002] or other organized structures related to flow along a boundary, for example, ejections and sweeps can be present [*Fer et al.*, 2004].

[18] We evaluated the LOW scaling both for ice stations and station D (Figure 5). The cases with ice-relative water speed (magnitude of vector difference between drift velocity and the average velocity from the shallowest two bins of the ADCP) greater or smaller than 0.20 m s^{-1} are examined separately. This is nearly equivalent to u_{*0} greater or smaller than ~1.4 cm s^{-1} because the surface friction speed and ice relative speed relation is tight (not shown). Given the 95% confidence intervals, we do not observe significant differences with respect to water speed in the stress-scaled profiles in the mixed or mixing layer. The distance from the ice is scaled by both D_{mixed} and D_{mixing}, separately. The latter shows a similar shape to that observed by *Lombardo and Gregg* [1989], where the scaled profile drops abruptly close to the base of the mixing layer. When the 0.05 normalized depth bin MLE values are averaged over the

mixed (mixing) layer ε is 4.5 (4) times that predicted by the LOW. This large ratio is mostly due to the enhanced dissipation within ~0.2–0.4 normalized distance from the ice. This is not the case for the open water station (dashed line in Figure 5b), where the increase with distance from the ice in the upper part of the water column is absent. The dissipation profile for the open water is in remarkable agreement with LOW with an average $\varepsilon/\varepsilon_s \sim 1.3$ within D_{mixing} (this excludes the last set after the storm event when no ADCP data were available). The most likely source for the increased dissipation in the drift stations in the upper half of the mixed layer is turbulence generated from an upstream source, for example, keels of pressure ridges.

4.2. Effect of Keels

[19] Using instrumented masts suspended in the boundary layer under drifting ice floes, direct measurements of Reynolds stresses and turbulent heat fluxes by the eddy-correlation method were previously reported [e.g., *McPhee*, 1992; *McPhee and Martinson*, 1994]. Besides the cases when turbulent fluxes did behave in a manner expected from a boundary layer near a rough wall, cases were also common when the Reynolds stress, hence local friction

Table 2. Average Vertical Temperature Gradient $\langle dT/dz \rangle$, Stratification $\langle N \rangle$, Vertical Eddy Diffusivity $\langle K_z \rangle$, and Heat Flux $\langle Q \rangle =$ rhoCp$\langle K_z \rangle \langle dT/dz \rangle$ in the Mixing Layer[a]

	Station A	Station B	Station C	Station D
	Averages Within the Mixing Layer, $|z|/D_{mixing} \leq 1$			
$\langle dT/dz \rangle$, $\times 10^{-3}$ °C m^{-1}	5 ± 15	7.3 ± 6.7	(-0.3 ± 0.7)	-2.6 ± 2.3
$\langle N \rangle$, $\times 10^{-3}$ s^{-1}	5.4 ± 6.5	6.5 ± 5	(2.5 ± 3.2)	(1.7 ± 1.4)
$\langle K_z \rangle$, $\times 10^{-2}$ m^2 s^{-1}	2.8 ± 5	2.9 ± 4	7.9 ± 12[b]	16 ± 16[b]
$\langle Q \rangle$, W m^{-2}	558	319	-87[b]	-1713[b]
$\langle K_z \rangle/(0.02u_{*0}^2/f)$	0.4	0.7	2.5[b]	2.8[b]
	Averages Within $0.9 \leq |z|/D_{mixing} \leq 1$			
$\langle dT/dz \rangle$, $\times 10^{-3}$ °C m^{-1}	37.4 ± 8.9	20 ± 4	1.6 ± 0.8	-5.0 ± 0.5
$\langle N \rangle$, $\times 10^{-3}$ s^{-1}	10.6 ± 5	6.8 ± 1.8	6.3 ± 3.2	2.2 ± 1
$\langle K_z \rangle$, $\times 10^{-2}$ m^2 s^{-1}	0.01 ± 0.01	0.09 ± 0.13	0.07 ± 0.08	0.72 ± 1
$\langle Q \rangle$, W m^{-2}	21	11.5	5	-149

[a]Average values are given as station mean ± one standard deviation, derived over the extent of the mixing layer and near the bottom of the mixing layer. For the averages within the mixing layer, the ratio $\langle K_z \rangle/(0.02u_{*0}^2/f)$ is also given. Vertical distance is positive upward, and a positive value of Q indicates an upward heat flux toward the ice; that is, ice gains heat. In the mixed layer, where the mean vertical gradients are weaker, the vertical gradient of temperature is not significantly greater than zero at 95% confidence for $[4-10] \times 10^{-4}$ °C m^{-1}, where values of N within $[10-30] \times 10^{-4}$ s^{-1} are zero at 95% confidence (the ranges cover the individual values for the four stations). The values not significantly different than zero are given in parentheses.
[b]Parameters are derived using values not significantly different than zero.

velocity, increased with distance from the ice bottom [*McPhee*, 2002]. For example, measurements when flow approached the instruments from an identified pressure ridge (with unknown keel depth), the friction speed profile showed enhanced values between $|z| \sim (0.3-0.6)/D_{mixed}$ [*McPhee*, 2002, Figure 5c], the signature of which is comparable to our observations (Figure 5). Another example is the case reported by *Skyllingstad et al.* [2003] where the local friction speed increased consistently with increasing vertical distance as recorded by instruments at $|z| \sim 0.16D_{mixed}$, $\sim 0.38D_{mixed}$ and $\sim 0.48D_{mixed}$ at the wake of a ~ 10 m deep keel ($h_{keel} \sim 0.4D_{mixed}$). These observations led *Skyllingstad et al.* [2003] to study the effects of keels in the turbulence exchange in the under-ice boundary layer. Using a large-eddy simulation of the latter mentioned case, they showed that the keel generated a turbulent wake region extending several hundreds of meters downstream from the keel, in good agreement with observations. The 10-m deep keel caused enhanced vertical mixing, increasing the heat flux fivefold from the background values.

[20] When the vertical distance from the ice is scaled with the keel depth, h_{keel}, the dissipation is observed to be larger than that predicted by LOW down to $(2-2.5)h_{keel}$, below which the dissipation profile approaches and agrees with the stress scaling (Figure 5c). We interpret this observation, in contrast with the open water station, as an influence of the keels on the turbulent structure in the under-ice mixed layer. In the lower half of the mixing layer depth, the effect of keels is negligible and average $\varepsilon/\varepsilon_s$ is within $1.6-1.8$, close to the observations of *Lombardo and Gregg* [1989]. Although based on a small data set, our observations indicate that the keels can enhance the dissipation levels (and momentum flux, assuming production balances dissipation) fourfold from levels expected from a wall layer within $2.5h_{keel}$, or the upper half of the mixed layer, in good agreement with other cases of direct measurements and modeling. Not having information on the orientation of

the keel, we cannot investigate the cases for along/across keel flow.

4.3. Heat Flux and Vertical Eddy Diffusivity

[21] Station averages are computed for the vertical eddy diffusivity, K_z, and heat flux, Q, and summarized in Table 2. The heat flux $Q = \rho C_P \langle dT/dz \rangle \langle K_z \rangle$ is calculated using density, ρ, and heat capacity, C_P, calculated with the station average θ and S tabulated in Table 1. An upper limit for K_z is estimated using Osborn's model $K_z = \Gamma \langle \varepsilon \rangle / \langle N^2 \rangle$ [*Osborn*, 1980] using the typical value $\Gamma = 0.2$ [*Moum*, 1996], a coefficient related to the efficiency of mixing. With the typical uncertainty of a factor 2 for ε, and accounting for variability of Γ, the eddy diffusivity derived using microstructure shear profilers in stratified waters cannot be more accurate than within a factor of $3-4$. For highly turbulent flows Reynolds analogy is expected to hold and diffusivities for salt, heat, buoyancy and momentum can all be considered equal within this uncertainty. In calculating K_z, the station average N is held constant to be representative of the average, background stratification (averaged over several semidiurnal periods), whereas the set-averaged ε is employed to derive the mean and variability of K_z.

[22] In the mixing layer, and particularly in the mixed layer, the vertical gradients of temperature and density, hence buoyancy frequency, are small and may not be reliably measured by our sensors. Because Osborn's model is not appropriate for nearly neutral stratification, care must be taken to evaluate K_z and Q. We calculate the vertical gradients as the slope of linear fits to 5-m moving windows of 10-cm resolution MSS temperature and density profiles. The values are retained only when the magnitude of the slope is greater than twice the standard error of the fit and are set to zero otherwise. The gradients are then ensemble averaged over the number of MSS sets during the stations. There is a low but significant background mean temperature gradient and stratification although the variability between sets is comparable to the station average. For reference, when calculated from the regression of temperature and

density against depth over the whole extent of the mixed layer D_{mixed}, the mean gradients are zero at 95% confidence for $\langle dT/dz \rangle = (0.4\text{-}1) \times 10^{-3}$ °C m^{-1} and $\langle N \rangle = (1-3) \times 10^{-3}$ s^{-1} (the ranges cover the individual values for the four stations). This suggests that in the mixing layer, the temperature gradient at C and the buoyancy frequency at both C and D may be questionable (Table 2) and the mean values for diffusivity and the heat flux in the mixing layer of these stations should be taken with caution. There is very strong vertical heat flux toward the ice in the mixing layers of A and B where average eddy diffusivities are nearly identical, and both these two stations have AW origin heat sources below the pycnocline.

[23] The averages within $0.9 \leq |z|/D_{mixing} \leq 1$, where the stratification is strong and significant, the values of K_z and Q are reliable. The heat flux is representative of that from the pycnocline toward the ice for the drift stations. The average heat flux is largest, ~ 21 W m^{-2}, at station A where the mixed layer temperatures are also the highest, consistent with warming of the f mixed layer by the AW from below. This value can be compared to the maximum heat flux of 27 W m^{-2} measured in the pycnocline on the northern flank of the Yermak Plateau at 2100 m water depth [*Padman and Dillon*, 1991]. Again consistent with the mixed layer temperature (close to the freezing point) is station C where the heat flux is only ~ 5 W m^{-2}. The eddy diffusivity at the base of the mixing layer ranges within $1-10 \times 10^{-4}$ m^2 s^{-1} under drifting ice. Diffusivity for the ice-free station is considerably larger for both the mixing layer column and the base of the mixing layer. The passage of the storm could possibly have increased the mixing here.

[24] The heat fluxes in the mixing layer are $10-30$ times that at the base of the mixing layer. This emphasizes that the small temperature gradients contribute significantly to the turbulent heat flux toward the ice given large vertical diffusivities. Although values of heat flux $300-500$ W m^{-2} may seem large, they are comparable to observations of *Ivanov et al.* [2003] who measured water/ice to air atmospheric heat fluxes in the Barents Sea MIZ (close to B in our study) during May in 1999. They describe large variations in the turbulent fluxes of sensible heat, reaching $300-500$ W m^{-2} during northerly winds. Furthermore, the ice cover at the drift stations is within $50-90\%$ (Table 1) and a large portion of the heat flux is thus expected to escape to the atmosphere without contributing to melting the ice. Comparable heat fluxes were reported in the MIZ of the Greenland Sea where direct measurements under drifting ice averaged to 388 W m^{-2} during a stormy summer day [*McPhee*, 1994]. Another set of observations supportive of large oceanic heat fluxes is the mixed layer temperatures recorded from drifting buoys of the North Pole Environmental Observatory, over the Yermak Plateau, which reached about 0.4 °C above the freezing point around day 50 of year 2003 (~ 3 months earlier in year than our observations in 2005) yielding heat flux estimates in excess of 100 W m^{-2} [*McPhee et al.*, 2003].

[25] In the under-ice boundary layer, in the absence of strong buoyancy flux, $\langle K_z \rangle$ was reported to be well-approximated by $0.02u_{*0}^2/f$ [*McPhee and Martinson*, 1994]. The ratio $\langle K_z \rangle / \langle 0.02u_{*0}^2/f \rangle$ is tabulated in Table 2, and the drift stations (as well as the ice-free station) suggest that the *McPhee and Martinson* [1994] relation, when averaged

across the mixing layer, captures the observed values of K_z within the large uncertainty. It is noted that this relation uses the neutral planetary length scale (and u_{*0} as velocity scale), to which the mixing was shown to be well correlated (Figure 10a, introduced later). Stabilizing buoyancy flux at stations A and B (section 4.4) will violate the assumption of neutral conditions. This is discussed in the next section. A relation involving local friction velocity and modified mixing length show slightly better agreement with the observations (section 4.4). The agreement between microstructure-inferred diffusivity and relations in the form of $u_* \lambda$ builds some confidence on our estimates using Osborn's model in weak stratification.

[26] Following *Turner* [1973], we can classify turbulent kinetic energy generating mechanisms as "external" (e.g., stress work at the surface for the oceanic surface mixing layer or that at the bottom boundary for bottom boundary layer) and "internal" (e.g., shear-induced mixing due to internal waves at the pycnocline). The average mixing throughout the under-ice mixing layer appears to be governed mainly by "external" parameters. The correlation between D_{mixing} and the stratified planetary scale was also significant (Figure 10b) which encourages a comparison between the average mixing at the base of the mixing layer ($0.9 \leq |z|/D_{mixing} \leq 1.1$) with $K_z \propto u_{*0}^2/(fN_{pyc})^{1/2}$ derived from this "external" length scale on dimensional grounds. The observed $\langle K_z \rangle$ at the base of the mixing layer is $(0.2-3) \times 10^{-3}$ and 10×10^{-3} times this scale for ice stations and ice-free station, respectively. The large range and scatter with no significant relation lead us to conclude that "internal" sources must partly contribute to mixing at the base of the mixing layer in the MIZ, where outer planetary scales alone are not sufficient to explain the processes. During moderate wind forcing, *Sundfjord et al.* [2007] found significant correlation between dissipation and thus diffusion rates within and below the pycnocline and current shear (variance) forced by tidal currents.

[27] The heat flux $Q_0 = \rho C_p \langle w'T' \rangle_0$ at the lower ice surface can be approximated using an exchange coefficient called the turbulent Stanton number, C_T, and the departure of the mixed-layer temperature from its freezing point as $Q_0 = \rho C_p C_T u_{*0}(T_\infty - T_f)$, where T_∞ is far-field mixed-layer temperature away from the ice [*McPhee*, 1992]. The Stanton number was found to be nearly constant (~ 0.0057) for a wide range of roughness Reynolds numbers [*McPhee et al.*, 1999]. Using $C_T = 0.0057$ and the station average u_{*0} and θ (for T_∞) Stanton number based heat flux estimates are 578, 224, 43 W m^{-2}, respectively for stations, A, B, and C (Table 3). The agreement with the observations is remarkable for A and B (Table 2). As discussed previously, the mean gradient at C is questionable and the calculated heat flux based on microstructure measurements can be in error. Nevertheless, the trend is similar between estimates from the two methods: heat flux for C is significantly lower than that for A and B. The comparison between our estimates of relatively large heat fluxes in the mixing layer and those from the independent method of *McPhee et al.* [1999] gives further confidence to our results.

4.4. Local Turbulence Closure and Effects of Stabilizing Buoyancy Flux

[28] Assuming that the boundary layer turbulence adjusts rapidly to changes in surface flux conditions and neglecting

Table 3. Inferred Surface Buoyancy Flux B_0, Monin-Obukhov Length L_{MO}, and Maximum Mixing Length Scale of the LTC, λ_{maxLTC}, for Drift Stations A–C

	Station A	Station B	Station C
Q_0, W m^{-2}	578	224	43
D_{mixed}, m	21	9	24
B_0,[a] $\times 10^{-7}$ W kg^{-1}	3.8	1.5	0.3
L_{MO}, m	80	81	281
λ_{maxLTC}, m	2.6	2.2	2.6
$\lambda_{maxLTC}/\lambda_{maxN}$	0.54	0.61	0.80
$\langle K_z \rangle / \lambda_{LTC} u_*$	0.6	1.1	2.6

[a]B_0 is estimated using ice-ocean interface heat flux, Q_0, and mean θ, S, and u_{*0} listed in Table 1.

advection of TKE, *McPhee* [1999] introduced the local turbulence closure (LTC) approach that incorporates a formulation of the turbulent mixing length, λ_{LTC}, in the oceanic mixed layer [*McPhee*, 1994], based on a similarity theory for the stable planetary boundary layer. For shear-driven turbulence, the eddy viscosity is calculated using local friction speed u_*, instead of u_{*0}, as $K = u_* \lambda_{LTC}$, where λ_{LTC} is allowed to follow the LOW ($\lambda = \kappa |z|$) until a maximum is reached, determined by the stability. For neutral or stable conditions the maximum mixing length is given by

$$\lambda_{max\,LTC} = \Lambda u_{*0} \eta^2 / |f|, \qquad (3)$$

where f is the Coriolis parameter, $\Lambda = 0.028$ and the stability factor is

$$\eta = \left[1 + \frac{\Lambda u_{*0}}{\kappa |f|} \frac{1}{R_c L_{MO}} \right]^{-1/2}, \qquad (4)$$

with the critical flux Richardson number, $R_c = 0.2$. The Monin-Obukhov length, $L_{MO} = u_{*0}^3/(\kappa B_0)$ is a measure of relative importance of stress and buoyancy flux. Buoyancy is expected to be important when L_{MO} is comparable with the other turbulent length scales in the flow [*Shay and Gregg*, 1986; *McPhee and Morison*, 2001]. For a complete description of λ_{LTC} and K in the mixed layer, friction velocity and buoyancy frequency at both boundaries, that is, at the ice-ocean interface and at the pycnocline, are needed since the stratification at the pycnocline will affect the mixing length. For a given u_{*0}, B_0 and T-S profile in the mixed layer, profiles of u_* and K can be estimated by an iterative technique [*McPhee*, 1999]. Here we do not apply iteration for generating u_* and K profiles but use the LTC approach (1) to show the expected change in the mixing length profile due to buoyancy effects and (2) to scale the observed dissipation with an estimate of shear production, $P_S = u_*^3/\lambda_{LTC}$, from the local friction speed assumed to follow the analytic solution of Ekman stress equation, $u_* = u_{*0} \exp\left[\sqrt{|f|/(2u_{*0}\lambda)}(z/2)\right]$.

[29] A crude estimate of the surface buoyancy flux induced by melting of sea ice can be made assuming that the upward oceanic heat flux at the ice-ocean interface is used entirely for melting at the interface, resulting in a salinity flux of $\langle w'S' \rangle_0 = (S - S_i) C_P \langle w'T' \rangle_0 / L_V$ [*McPhee*, 1994]. Here, S and S_i are the mixed layer and sea ice salinities, respectively, and L_V is the latent heat of fusion for saline ice ($\sim$301 kJ kg^{-1} for $-2°C$ ice with $S_i = 4$). The buoyancy flux at the interface is $B_0 = \langle w'b' \rangle_0 = g(\beta \langle w'S' \rangle_0$
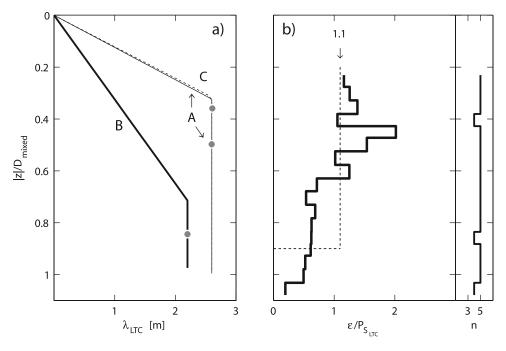
$- \alpha \langle w'T' \rangle_0)$ where g is the gravitational acceleration, α is the thermal expansion coefficient and β is the haline contraction coefficient. Using $S_i = 4$, S values from Table 1 and Stanton-number-derived $\langle w'T' \rangle_0 = Q_0/\rho\,C_P$, we estimate B_0 (Table 3). The buoyancy flux at A and B is $O(10^{-7})$ W kg^{-1}, 1 order of magnitude greater than that at C. In response to B_0, we expect reduction in the maximum mixing length in the mixed layer, through equations (3) and (4). Results are summarized in Table 3 and Figure 6. λ_{maxLTC} is 0.5 (station A) to 0.8 (station C) times the mixing length expected from the maximum length scale in a neutral planetary boundary layer, $\lambda_{maxN} \approx 0.03\,u_{*0}/f$ [*McPhee and Morison*, 2001]. When values of Q averaged within D_{mixing} listed in Table 2 are taken as Q_0 (instead of Stanton number based estimates), results for station A remain identical whereas $\lambda_{maxLTC} = 2$ m at station B.

[30] The local shear production, $P_S = u_*^3/\lambda_{LTC}$, captures the variability of the mean dissipation profiles within a factor of 2, comparable to the measurement uncertainty, and $\varepsilon/P_{S_{LTC}} = 1.1$ when averaged within $|z|/D_{mixed} \le 0.9$ (Figure 6b). We repeat that our application of LTC will not be valid as the pycnocline is approached and the actual u_* profile, hence P_S, can be different than the assumed analytic solution of the Ekman stress equation. Nevertheless, this scaling captures the salient features of the observations and is a better approximation compared to LOW. The average dissipation is less ($0.9 P_{S_{LTC}}$) when the portion affected by the keel is removed. Because we can only make a crude estimate of B_0 from station mean values, the scaling of ε is done only for the station mean profiles (instead of set mean profiles). When averaged between $0.2 \le |z|/D_{mixed} \le 0.9$ (lower and upper limits imposed by the observations closest to the ice and by the proximity to the pycnocline, respectively), $P_{S_{LTC}}$ is 8 (station A) to 25 (station C) times B_0, hence shear production dominates. The vertical transport terms in the TKE, assumed negligible throughout this study, cannot be assessed using our data set. *McPhee* [2004], using yearlong SHEBA data, showed that the average imbalance between shear production and dissipation measured at two levels sufficiently away from the boundary could be explained by the divergence of vertical TKE flux. The approximate balance between ε and $P_{S_{LTC}}$ reported here may be due to possible cancelling of buoyancy flux and transport terms and/or a deviation of the assumed u_* profile from the real one in favor of the ε-P_S balance. Nevertheless, the scaling accounts for the suppression of the mixing length by stabilizing buoyancy forces and employs a representative profile for u_* giving good estimates of the mean dissipation in the mixed layer above the pycnocline.

[31] A comparison between the inferred eddy diffusivity from the Osborn model and eddy viscosity from LTC suggests overall agreement, slightly better than bulk diffusivity for neutral conditions suggested by *McPhee and Martinson* [1994] (compare Tables 2 and 3). A detailed discussion on comparing dissipation-derived diffusivity and $K \propto u_*\lambda$ is not warranted because of the contradictory assumptions in each approach.

4.5. Modified Law of the Wall

[32] Observations near the oceanic bottom-boundary layers typically adhere to LOW when inferred from near-

Figure 6. Vertical profiles of (a) mixing length for drift stations A (thin line), B (thick line), and C (dashed line) and (b) average dissipation scaled by the shear production, P_S, estimated using the local turbulence closure (LTC) model [*McPhee*, 1999]. Vertical distance from the ice is normalized by the mixed layer depth, D_{mixed}. Gray circles in Figure 6a mark $|z|/D_{mixing} = 0.3$, for reference. The profiles are derived from station mean values in $|z|/D_{mixed} = 0.05$ unit bins, and the number of data points, n, used in averaging ε is shown in the last panel. Scaled dissipation within $|z|/D_{mixed} \leq 0.9$ is 1.1 (vertical dashed line in Figure 6b).

bottom measurements (within several m from the bottom). This is occasionally the case also for the upper ocean boundary layer [*Gargett*, 1989; *Lombardo and Gregg*, 1989], and more frequently, for the under-ice boundary layer. Farther from the boundary the velocity gradient typically decreases with distance from the boundary at a rate greater than that predicted by LOW. In a recent study, *Perlin et al.* [2005], propose a modified version of LOW where the mixing length-scale asymptotes from a linearly varying profile near the boundary to the Ozmidov length, L_O, at the top, consistent with suppression of the length of turbulent eddies by the stratification capping the quasi-homogeneous, mixed layer. They find that observations from several data sets agree very well when scaled with the LOW modified by the empirical mixing length

$$\lambda = \kappa |z| \left(1 - \frac{|z|}{h_d}\right). \tag{5}$$

For a stratified boundary layer h_d is chosen such that the mixing length approaches L_O near the mixed layer depth, that is, $h_d = D_{mixed}/[1-(L_O/\kappa D_{mixed})]$. This is consistent with the observations of *McPhee and Martinson* [1994], who estimated mixing length in a near-neutral under-ice mixing layer in drifting ice, showing that $\lambda = \kappa |z|$ (LOW) does not hold for depths $> \sim 4$ m (note the resemblance between the modified LOW exemplified in Figure 7b here and their Figure 4a).

[33] In near neutral stratification L_O is not a relevant parameter but as the stratified base of the mixed layer is approached, it is representative of the maximum length

turbulent eddies may achieve. We observe $L_O \sim 4$ m at about half the mixing layer depth, decreasing to $0.3-1$ m at the base of D_{mixing} (Figure 7). We chose to average L_O within $0.9 \leq |z|/D_{mixing} \leq 1.1$ for each MSS set to evaluate the modified LOW. The resulting length-scale curves normalized by mixing layer depth for each set are shown in Figure 7b and contrasted to LOW. The modified LOW effectively reduces the length scale in the lower half of the mixing layer. The range of λ associated with the modified LOW is consistent with the maximum length scale in a neutral planetary boundary layer, $\lambda_{maxN} \approx 0.03 \, u_{*0}/f$ [*McPhee and Morison*, 2001].

[34] The stress scaling using the modified LOW length scale is applied to dissipation profiles and shown in Figure 8. Also shown is the standard LOW scaling (Figure 8, gray line) for comparison. Because the stress scaling of dissipation is most sensitive to u_{*0} (to the third power), the modification of λ significantly affects the scaled profile only in the lower half of the mixing layer, where λ considerably deviates from LOW. When the vertical distance from the ice is scaled by D_{mixing}, $\langle \varepsilon/\varepsilon_{smod} \rangle \sim 1.75$, on the average, performs better than the LOW ($\langle \varepsilon/\varepsilon_s \rangle \sim 4$), but overestimates the observed levels on the lower half of the mixing layer where the standard LOW appears more favorable. If the modified LOW is a better model for the under-ice mixing layer, as it was shown to be for oceanic bottom boundary layers [*Perlin et al.*, 2005], the discrepancy between the observations and the model can be due to unresolved issues concerning the transport of turbulent kinetic energy and possible use of a part of turbulent kinetic energy to radiate internal waves at the base of the mixed
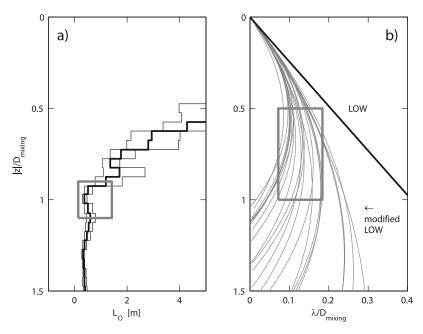
Figure 7. Profiles of (a) Ozmidov length scale $L_O = (\varepsilon/N^3)^{1/2}$ MLE values (thick lines) and 95% confidence intervals (thin lines) and (b) mixing length scale λ normalized by the mixing layer depth for law of the wall (LOW, thick line) and modified law of the wall (shaded curves). In both Figures 7a and 7b, ordinate is the distance from ice scaled by D_{mixing}. Very large values of L_O in the nearly neutral stratification in the upper half of D_{mixing} are irrelevant and not shown. The horizontal extent of the shaded box in Figure 7a covers the total range of individual values for 23 mean profiles over $|z|/D_{mixing} = 0.9-1.1$ (vertical extent of the box) used in the calculation of the modified-LOW length scale. The horizontal extent of the box in Figure 7b is the range of maximum mixing length in the rotational outer boundary layer, $\lambda_{max} \approx 0.03\ u_{*0}/f$, derived using local f and friction velocity for each MSS set (the vertical extent is arbitrary).

layer [*Linden*, 1975]. If this is the case, the agreement with the standard LOW away from the keels would be fortuitous.

4.6. Column-Integrated Dissipation

[35] The rate of dissipation of turbulent kinetic energy, ε, is an important component of the mixed layer energy budget. The integrated dissipation in the mixed layer

$$\varepsilon_1 = \int_0^{D_{mixed}} \rho\varepsilon(z)dz \quad \left[W\ m^{-2}\right] \tag{6}$$

is well-correlated with and accounts for a fraction of the energy flux in the atmospheric boundary layer. In ice-free conditions, a large fraction of the rate of working of wind stress at 10 m, E_{10}, is dissipated in air and between 4–9% of E_{10} is estimated to penetrate the air-sea interface ($E_0 \equiv \rho u_{*0}^3$) [*Richman and Garrett*, 1977] and only 0.1–0.2% of E_{10} is used to increase the potential energy of a deepening mixed layer [*Denman and Miyake*, 1973]. When the forcing is dominated by wind stress, *Oakey and Elliott* [1982] reported $\varepsilon_I \approx 0.01E_{10}$ (or $\varepsilon_I \approx 6.5E_0$). Comparable result ($\varepsilon_I \approx (4 \pm 1)E_0$) was obtained by *Dewey and Moum* [1990], who integrated ε through the mixing layer. In the upper mixed layer in the North Atlantic, recent measurements bounded the ratio ε_I/E_{10} between 0.03–0.07 [*Lozovatsky et al.*, 2005]. When the surface is ice-covered, the wind-stress-related turbulent production is due to the rate of working of

stress under the ice. Using an estimate of $E_0 \approx C_D^{3/2}U^3$ with drag coefficient of $C_D = 0.005$ and ice-relative current, U, at 300 m depth, *Padman and Dillon* [1991] obtained $\varepsilon_I \approx 2.4E_0$ for U > 0.05 m s^{-1} under the drifting pack ice near the Yermak Plateau. In the above cited studies, ε_I is measured by microstructure profilers with shear probes and the unreliable measurements in the upper 5–8 m of the mixed layer were accounted for either by extending the uppermost reliable measured value to the surface or applying a law of the wall model to the dissipation profile. *Padman and Dillon* [1991] state that the relatively low value of ε_I/E_0 compared to open water observations may be due to the unique nature of ice-ocean momentum transfer and/or the consequences of choosing the drag coefficient, ice-relative current level, and extrapolation of ε.

[36] Using the integrated dissipation over the mixing layer depth, we find significant correlation of ε_I with E_0 and E_{10}, for both ice-drift and open water stations (Figure 9). In evaluating ε_I, we assume LOW is applicable for the uppermost 5–8 m. This range is less than the depth where the LTC attains its maximum mixing length deviating from LOW (compare D_{mixed} in Table 3 and Figure 6a). For the drift stations, $E_0 = \rho u_{*0}^3$ is calculated with u_{*0}, friction speed, estimated using the steady state force balance as described previously. For the ice-free station, $u_{*0} = [(\rho_a/\rho_w)C_DU_{10}^2]^{\frac{1}{2}}$. The least squares fit yields $\varepsilon_I/E_0 \approx 9.9\ (\pm 2)$, when each parameter varies more than two decades. The open water observations do not show a significantly differ-
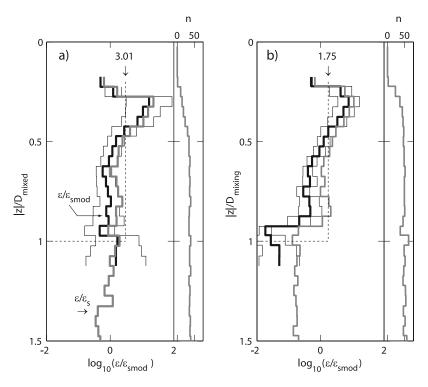
Figure 8. Profiles of dissipation rate ε normalized by the modified law of the wall $\varepsilon_{smod} = u_{*0}^3/\lambda$ with λ from equation (5) (black lines), where the distance from ice $|z|$ is scaled (a) by the mixed layer depth, D_{mixed}, and (b) by the mixing layer depth, D_{mixing}. The MLE values (black lines) and 95% confidence intervals are shown for $|z|/D_{mixing} = 0.05$ bins. There are typically $\sim$50 data points, n, averaged in each normalized depth bin of the lower half of the mixed and mixing layers (narrow adjacent panels). The average of the standard LOW scaling (over both cases of ice relative speed in Figure 5) is shown for reference (gray lines).

ent pattern and we include all data in the regression. This ratio is larger than previous open water observations and appears inconsistent with low inferred values under ice [*Padman and Dillon*, 1991]. The drag coefficient chosen by *Padman and Dillon* [1991] is approximately twice the C_D used in this study, and because $E_0 \propto C_D^{3/2}$, a factor of $\sim$3 discrepancy may be expected. Furthermore, their measurements were conducted under pack ice and a dense ice cover is expected to reduce effective transfer of momentum from wind to water. In the previous section it is shown that the keels significantly enhance dissipation in the upper half of D_{mixed}, which in turn would lead to an increase in ε_I and ε_I/E_0. These factors can partly explain why ε_I/E_0 in our survey is larger than that reported for previous ice-free studies. Consistent with this statement, it can be noted that the ice-free data points from our survey would yield a slightly lower ratio, albeit statistically insignificant, than ice-drift stations alone (Figure 9). Given the uncertainties, sensitivity to the choice of parameters and not being able to assess the details of transfer from E_0 to ε_I, we can only make the point that our data set indicates a significant correlation between the column-integrated dissipation in the mixing layer and the work done by the stress at the surface, at a rate not inconsistent with previously reported values.
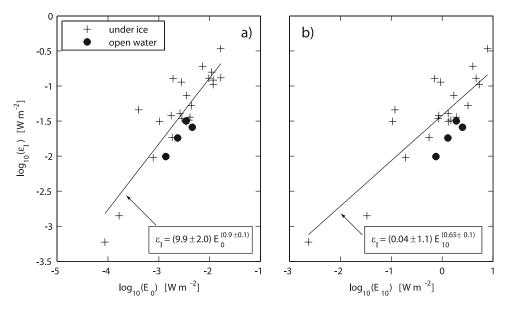
[37] Because E_{10} is a more conventionally measured parameter $\varepsilon_I \propto E_{10}$ dependence is often preferable. Previous observations support a linear relation with constant of proportionality in the range 0.01–0.07 [*Oakey and Elliott*,

1982; *Lozovatsky et al.*, 2005]. Our observations suggest that the power on E_{10} is significantly less than unity (Figure 9b) for partially ice-covered sea. This might be owing to an efficient reduction in the energy transfer between the wind and under-ice boundary layer related to the presence of ice, or to the choice of C_D.

4.7. Mixed Layer Depth, Mixing Layer Depth, and Entrainment

[38] It is often desirable to derive relations between surface forcing and the mixed layer depth and its deepening. When stress is the dominant forcing mechanism the relevant velocity scale is the friction speed u_{*0} and, in a neutral boundary layer, the outer length scale (away from very near the surface) is the planetary length scale u_{*0}/f. The length scale will be modified in the presence of significant buoyancy fluxes (section 4.4). A stratified planetary length scale, $u_{*0}/(fN_{pyc})^{1/2}$ can also be a good indicator of the mixed layer depth evolution after strong stress forcing [*Pollard et al.*, 1973; *Lentz*, 1992; *Lozovatsky et al.*, 2005]. N_{pyc} is the buoyancy frequency at the pycnocline, here calculated as the mean N between the base of the mixed layer and the base of the pycnocline.

[39] Zero-lag correlation coefficients, r, between D_{mixed}, D_{mixing} and planetary length scales are tabulated in Table 4. The values of r obtained using the mixed layer depths and the length scale for neutral conditions are either not significantly different than zero or low. When the mixing length is modified by factor $A = \lambda_{maxLTC}/\lambda_{maxN}$ (Table 3), the

Figure 9. The dissipation integrated over the mixed layer, ε_I, versus (a) under-ice energy flux rate, E_0, (b) wind work at 10 m, E_{10}, for ice stations (crosses) and open water (solid circles). The upper $5-8$ m of the dissipation profile not reliably measured by our sampling is approximated using LOW. The intercept and exponent of the linear fit are indicated with ± standard errors.

expected reduction in maximum mixing length due to estimated buoyancy flux at each station, the correlation coefficients consistently increase.

[40] We find the mixing length D_{mixing} to be significantly correlated with both neutral and stratified planetary length scales. For the reasons that the LTC derived λ_{max} values will not be valid near the pycnocline and D_{mixing} typically extends below the pycnocline, we did not account for the effects of the buoyancy flux in D_{mixing} correlations. Implementing the assessed ice cover and keel depth values, we find slightly higher correlations using D_{mixing}, however, not conclusively more significant than using the standard planetary scales alone. The regressions of D_{mixing} against neutral and stratified planetary scales are shown in Figure 10. When the intercept is set to zero, $D_{mixing} = 0.23\ u_{*0}/f$ and $D_{mixing} = 1.5\ u_{*0}/(fN_{pyc})^{1/2}$ with slightly lower correlation coefficients of 0.65 and 0.62, respectively.
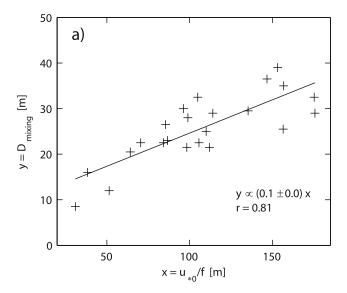
The ratio $D_{mixing}/[u_{*0}/(fN_{pyc})^{1/2}]$ is in good agreement with the range $1.3-1.9$ derived from both observations and numerical models (for summary, see *Lozovatsky et al.* [2005]). In the upper mixed layer in the North Atlantic, *Lozovatsky et al.* [2005] obtained a tight relation, $D_{mixed}/(u_{*0}/f) \sim 0.44$ when D_{mixed} was lagged 12 hours. Because wind has to work for a period to effectively erode the existing stratification in deep mixed layers, higher correlations are observed between D_{mixed} and u_{*0} when lagged $\sim5-12$ hours [*Lentz*, 1992; *Lozovatsky et al.*, 2005]. In this study, relatively low values of r obtained using D_{mixed} could perhaps improve with an appropriate time lag, which cannot be evaluated with our drift stations.
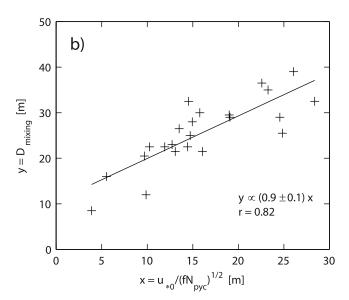
[41] The mixed layer deepens by entraining stratified water across its base. For cases when turbulent entrainment is stress driven, power laws in terms of a bulk Richardson number, $Ri_o = D_{mixed}\Delta b/u_{*0}^2$, where Δb is the buoyancy

Table 4. Correlation Between Mixed Layer Depth D_{mixed}, Mixing Layer Depth D_{mixing}, and Chosen Parameters[a]

Parameter 1	Parameter 2	Correlation Coefficient, r
u_{*0}/f, Au_{*0}/f	D_{mixed}	(0.35), 0.61
u_{*0}/f	D_{mixing}	0.81
$u_{*0}/(h_{keel}f)$, $Au_{*0}/(h_{keel}f)$	D_{mixed}	0.56, 0.70
$u_{*0}/(h_{keel}f)$	D_{mixing}	0.8
$(u_{*0}/I)/(h_{keel}\ f)$, $A(u_{*0}/I)/(h_{keel}\ f)$	D_{mixed}	0.48, 0.70
$(u_{*0}/I)/(h_{keel}\ f)$	D_{mixing}	0.83
$u_{*0}/(N_{pyc}\ f)^{1/2}$, $Au_{*0}/(N_{pyc}\ f)^{1/2}$	D_{mixed}	(0.35), 0.60
$u_{*0}/(N_{pyc}\ f)^{1/2}$	D_{mixing}	0.82
$(u_{*0}/I)/(N_{pyc}\ f)^{1/2}$, $A(u_{*0}/I)/(N_{pyc}\ f)^{1/2}$	D_{mixed}	(0.31), 0.50
$(u_{*0}/I)/(N_{pyc}\ f)^{1/2}$	D_{mixing}	0.79

[a]Parameter u_{*0} is the friction velocity under ice, h_{keel} is the keel depth (from sea surface), I is the ice coverage in percent, N_{pyc} is the buoyancy frequency between the mixed layer and the base of the pycnocline. The number of data points is 23, giving a correlation coefficient significantly greater than zero $r \sim 0.4$ at 95% confidence. The values of r not significantly different than zero are given in parentheses. The correlations between D_{mixed} are also derived after modifying parameter 1 by $A = \lambda_{maxLTC}/\lambda_{maxN}$ (Table 3), the expected reduction in maximum mixing length due to estimated buoyancy flux at each station.
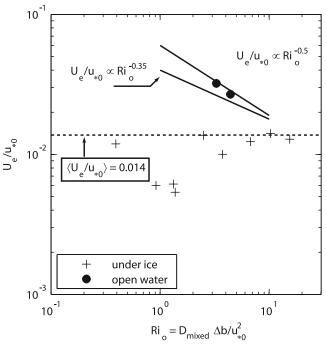
Figure 10. Regression of mixing layer depth, D_{mixing}, against (a) outer neutral planetary length scale, u_{*0}/f, and (b) stratified planetary length scale, $u_{*0}/(fN_{pyc})^{1/2}$. The slope (± standard error) of the linear least squares fit (with nonzero intercept) is indicated together with the correlation coefficient, r. When intercept is set to zero slopes are 0.23 ($r = 0.65$) and 1.5 ($r = 0.62$) for Figure 10a and 10b, respectively.

(density times the gravitational acceleration) jump below the mixed layer depth D_{mixed}, have been suggested in literature. When the rate of change of depth of a deepening mixed layer is defined as entrainment speed, U_e, a relation of the form $U_e/u_{*0} \propto Ri_o^m$ can be suggested where $m \sim -0.5$ [*Price*, 1979], or $m \sim -0.35$ [*Mellor and Strub*, 1980] (as inferred by *Nagai et al.* [2005]). Recently, *Nagai et al.* [2005] reported on field and numerical study results on entrainment laws for the surface mixed layer of a lake where they propose a stress-buoyancy combined scaling when both forces are at play. On the other hand, *Kantha et al.*

[1977] emphasize that the power m should vary with Ri_o such that for very turbulent flows $Ri_o \to 0$, $m \sim 0$ and for very stratified flow $m \sim \infty$ (see also the thorough review by *Nagai et al.* [2005]). We use our scarce observations from the times when D_{mixed} was deepening to evaluate this dependency. U_e is estimated by the slope of the linear fit to the mixed layer depth against time, Δb at the base of the mixed layer is obtained as the buoyancy at the first point from 0.5 m CTD bins below D_{mixed} minus the depth mean buoyancy within D_{mixed}. The values of Ri_o are remarkably low, implying a turbulent regime, with no significant relation with the normalized entrainment speed (Figure 11). This is consistent with m approaching zero for low values of Ri_o, implying $U_e/u_{*0} \sim$ constant (with an average value of 0.014, here). We cannot rule out the fact that the apparent scatter and the lack of clear relation between U_e/u_{*0} and Ri_o can be as a consequence of the large natural variability on a variety of scales, including factors such as wind stress curl from passing low-pressure systems that may act to lift the pycnocline [*McPhee et al.*, 2005]. The available data points from open water are suggestive of power law dependence close to -0.5, but this is certainly not conclusive.

5. Summary and Concluding Remarks

[42] Measurements of turbulent kinetic energy dissipation and small-scale hydrography from the under-ice boundary layer in the marginal ice zone of the Barents Sea have been analyzed with emphasis on the coupling between external

Figure 11. Normalized entrainment speed, U_e/u_{*0}, versus bulk Richardson number, Ri_o, derived from observations when the mixed layer was deepening. Drift stations do not show any apparent trend with Ri_o and scatter around a mean of 0.014. Relevant power laws reported in the literature are shown for reference. Two data points available from the ice-free station agree fairly well with the $Ri_o^{-0.5}$ power law.

forcing, processes within the mixing layer, effect of stabilizing buoyancy flux encountered by melting of sea ice, and deepening of and entrainment into the mixed layer. Here we summarize our conclusions emphasizing the caveats that vertical transport in the local TKE balance is neglected and the limited measurements were made during the drift (except D) across a frontal system with horizontally non-homogeneous hydrography which can significantly influence our inferences of the mixed and mixing layer dynamics. Furthermore, the air-ice/ice-water drag coefficient remains an important parameter the choice of which can significantly influence the results.

[43] During the survey, significant buoyancy fluxes were estimated for stations A and B; however, shear production by the stress at the surface or under the ice dominated. The wind stress scaling using the LOW underestimated the mixing layer depth-averaged dissipation with a factor of 4. This was suggested to be associated with the enhanced dissipation induced by the pressure-ridge keels for two reasons: (1) a reference open water stations agreed well with the LOW and (2) the departure from LOW was large within 2.5 keel depth below which (or in the lower half of the mixing layer) the agreement with LOW was acceptable within the uncertainties. A modified LOW model yields results, when scaled with the observations, which are close to values reported previously but with a skewed dissipation profile. In the lower half of the mixing layer the modified model predicts larger values than observed. The mixing length associated with the modified model is significantly reduced away from the boundary and is within the range of maximum mixing length expected in a rotational outer boundary layer. We cannot conclude as to whether this modified scaling, shown to be appropriate for bottom boundary layers, is advantageous also for use at the ice-ocean boundary.

[44] The salient features of the observations and variability of dissipation in the mixed layer were better captured using the local turbulence closure (LTC) approach [*McPhee*, 1999], which accounts for the change in the mixing length profile due to buoyancy fluxes and employs local friction speed in deriving shear production and eddy viscosity. We simply used the analytic solution of Ekman stress equation for a representative u_* profile and a crude estimate of the surface buoyancy flux assuming that the upward oceanic heat flux at the ice-ocean interface is used entirely for melting. The maximum mixing length in the mixed layer reduced by factor 0.5–0.8 than that expected in a neutral planetary boundary layer. The local shear production captured the variability of the mean dissipation profiles and approximately balanced the mixed layer average within the measurement uncertainty.

[45] Observed dissipation integrated over the mixing layer is strongly correlated with work done by stress under the ice with the relation $\varepsilon_I/E_0 \approx 9.9$ (± 2). The correlation was also significant with the wind work at 10 m height but the relation was $\varepsilon_I \propto E_{10}^{(0.65\pm0.1)}$, suggesting that energy transfer between the wind and under-ice boundary layer is effectively reduced compared to open water observations in the literature (where $\varepsilon_I \propto E_{10}$). The low correlation between the mixed layer depth and length scale for neutral conditions significantly increased when the reduction in the mixing length due to buoyancy fluxes was accounted for. The

highest correlations, however, were found between the mixing layer depth and the outer neutral planetary length u_{*0}/f and the stratified planetary length scale $u_{*0}/(fN_{pyc})^{1/2}$. The eddy diffusivities inferred from microstructure data were high ($O(10^{-2})m^2\ s^{-1}$), in rough agreement with $K \propto u_*\lambda$ relations. At ice stations where cold surface water overlays warm water of Atlantic origin the vertical heat fluxes were considerable. Fluxes of $300-500$ W m^{-2} were inferred for stations A (where the AW is transported by the West Spitsbergen Current at the northern shelf break of Svalbard) and B (just north of the central Barents Sea Polar Front). These fluxes were found to compare well with those obtained from an independent parameterization [*McPhee et al.*, 1999]. Inferred bulk Richardson number, Ri_o, values were low, in the range $0.5-20$, as expected from a highly turbulent regime. In the observed range of Ri_o, the rate of deepening of the mixing layer depth was found to be a nearly constant fraction ($0.5-1.5\%$) of the friction speed, and independent of Ri_o.

[46] The effect of keels on turbulence under the ice merits further studies and the assessment of the under-ice topography and roughness remains a challenge. Positively buoyant microstructure profilers deployed in rising mode with a guide pulley suspended at a depth below the mixed layer and with a probe guard large enough to allow for approaching the under-ice surface as close as $5-10$ cm can help to resolve the turbulence structure very close to the ice.

References

Agrawal, Y. C., E. A. Terray, M. A. Donelan, P. A. Huang, A. J. Williams III, W. M. Drennan, K. K. Kahma, and S. A. Kitagorodski (1992), Enhanced dissipation of kinetic energy beneath surface waves, *Nature*, *359*, 219–220.

Baker, M. A., and C. H. Gibson (1987), Sampling turbulence in the stratified ocean: Statistical consequences of strong intermittency, *J. Phys. Oceanogr.*, *17*, 1817–1836.

Bourke, R. H., A. M. Weigel, and R. G. Paquette (1988), The westward turning branch of the West Spitsbergen Current, *J. Geophys. Res.*, *93*, 14,065–14,077.

Brainerd, K. E., and M. C. Gregg (1995), Surface mixed and mixing layer depths, *Deep Sea Res., Part I*, *42*, 1521–1543.

Denman, K. L., and M. Miyake (1973), Upper layer modification at ocean station Papa: Observations and simulation, *J. Phys. Oceanogr.*, *3*, 185–196.

Dewey, R. K., and J. N. Moum (1990), Enhancement of fronts by vertical mixing, *J. Geophys. Res.*, *95*, 9433–9445.

Falk-Petersen, S., H. Hop, W. P. Budgell, E. N. Hegseth, R. Korsnes, T. B. Loyning, J. B. Orbaek, T. Kawamura, and K. Shirasawa (2000), Physical and ecological processes in the marginal ice zone of the northern Barents Sea during the summer melt period, *J. Mar. Syst.*, *27*, 131–159.

Fer, I. (2006), Scaling turbulent dissipation in an Arctic fjord, *Deep Sea Res., Part II*, *53*, 77–95.

Fer, I., M. G. McPhee, and A. Sirevaag (2004), Conditional statistics of the Reynolds stress in the under-ice boundary layer, *Geophys. Res. Lett.*, *31*, L15311, doi:10.1029/2004GL020475.

Gargett, A. E. (1989), Ocean turbulence, *Annu. Rev. Fluid Mech.*, *21*, 419–451.

Guest, P. S., J. W. Glendening, and K. L. Davidson (1995), An observational and numerical study of wind stress variations within marginal ice zones, *J. Geophys. Res.*, *100*, 10,887–10,904.

Ingvaldsen, R. B., L. Asplin, and H. Loeng (2004), The seasonal cycle in the Atlantic transport to the Barents Sea during the years 1997–2001, *Cont. Shelf Res.*, *24*, 1015–1032.

Ivanov, B. V., S. Gerland, J.-G. Winther, and H. Goodwin (2003), Energy exchange processes in the marginal ice zone of the Barents Sea, Arctic Ocean, during spring 1999, *J. Glaciol.*, *49*, 415–419.

Kaltin, K., L. G. Anderson, K. Olsson, A. Fransson, and M. Chierici (2002), Uptake of atmospheric carbon dioxide in the Barents Sea, *J. Mar. Syst.*, *38*, 31–45.

Kantha, L. H., O. M. Phillips, and R. Azad (1977), On turbulent entrainment at a stable density interface, *J. Fluid Mech.*, *79*, 753–768.

Lentz, S. J. (1992), The surface boundary layer in coastal upwelling regions, *J. Phys. Oceanogr.*, *22*, 1517–1539.

Linden, P. F. (1975), The deepening of a mixed layer in a stratified flow, *J. Fluid Mech.*, *71*, 385–405.

Lombardo, C. P., and M. C. Gregg (1989), Similarity scaling of viscous and thermal dissipation in a convecting boundary layer, *J. Geophys. Res.*, *94*, 6273–6284.

Lozovatsky, I., M. Figueroa, E. Roget, H. J.S. Fernando, and S. Shapovalov (2005), Observations and scaling of the upper mixed layer in the North Atlantic, *J. Geophys. Res.*, *110*, C05013, doi:10.1029/2004JC002708.

McPhee, M. G. (1990), Small scale processes, in *Polar Oceanography*, edited by W. O. J. Smith, pp. 287–334, Elsevier, New York.

McPhee, M. G. (1992), Turbulent heat flux in the upper ocean under sea ice, *J. Geophys. Res.*, *97*, 5365–5379.

McPhee, M. G. (1994), On the turbulent mixing length in the oceanic boundary layer, *J. Phys. Oceanogr.*, *24*, 2014–2031.

McPhee, M. G. (1999), Parameterization of mixing in the ocean boundary layer, *J. Mar. Syst.*, *21*, 55–65.

McPhee, M. G. (2002), Turbulent stress at the ice/ocean interface and bottom surface hydraulic roughness during the SHEBA drift, *J. Geophys. Res.*, *107*(C10), 8037, doi:10.1029/2000JC000633.

McPhee, M. G. (2004), A spectral technique for estimating turbulent stress, scalar flux magnitude, and eddy viscosity in the ocean boundary layer under pack ice, *J. Phys. Oceanogr.*, *34*, 2180–2188.

McPhee, M. G., and D. G. Martinson (1994), Turbulent mixing under drifting pack ice in the Weddell Sea, *Science*, *263*, 218–221.

McPhee, M. G., and J. H. Morison (2001), Under-ice boundary layer, in *Encyclopedia of Ocean Sciences*, edited by J. H. Steele et al., pp. 3069–3076, Elsevier, New York.

McPhee, M. G., C. Kottmeier, and J. H. Morison (1999), Ocean heat flux in the central Weddel Sea in winter, *J. Phys. Oceanogr.*, *29*, 1166–1179.

McPhee, M. G., T. Kikuchi, J. H. Morison, and T. P. Stanton (2003), Ocean-to-ice heat flux at the North Pole environmental observatory, *Geophys. Res. Lett.*, *30*(24), 2274, doi:10.1029/2003GL018580.

McPhee, M. G., R. Kwok, R. Robins, and M. Coon (2005), Upwelling of Arctic pycnocline associated with shear motion of sea ice, *Geophys. Res. Lett.*, *32*, L10616, doi:10.1029/2004GL021819.

Mellor, G. L., and P. T. Strub (1980), Similarity solutions for the stratified turbulent Rayleigh problem, *J. Phys. Oceanogr.*, *10*, 455–460.

Moum, J. N. (1996), Efficiency of mixing in the main thermocline, *J. Geophys. Res.*, *101*, 12,057–12,069.

Moum, J. N., M. C. Gregg, R. C. Lien, and M. E. Carr (1995), Comparison of turbulent kinetic energy dissipation rate estimates from two ocean microstructure profilers, *J. Atmos. Oceanic Technol.*, *12*, 346–366.

Nagai, T., H. Yamazaki, H. Nagashima, and L. H. Kantha (2005), Field and numerical study of entrainment laws for surface mixed layer, *Deep Sea Res., Part II*, *52*, 1109–1132.

Oakey, N. S., and A. J. Elliott (1982), Dissipation within the surface mixed layer, *J. Phys. Oceanogr.*, *12*, 171–185.

Osborn, T. R. (1980), Estimates of the local rate of vertical diffusion from dissipation measurements, *J. Phys. Oceanogr.*, *10*, 83–89.

Padman, L., and T. Dillon (1991), Turbulent mixing near the Yermak Plateau during the coordinated Eastern Arctic Experiment, *J. Geophys. Res.*, *96*, 4769–4782.

Perlin, A., J. N. Moum, J. M. Klymak, M. D. Levine, T. Boyd, and P. M. Kosro (2005), A modified law-of-the-wall applied to oceanic bottom boundary layers, *J. Geophys. Res.*, *110*, C10S10, doi:10.1029/2004JC002310.

Pfirman, S. L., D. Bauch, and T. Gammelsrød (1994), The Northern Barents Sea: Water mass distribution and modification, in *The Polar Oceans and Their Role in Shaping the Global Environment: The Nansen Centennial Volume, Geophys. Monogr. Ser.*, vol. 85, edited by O. M. Johannessen et al., pp. 77–94, AGU, Washington, D. C.

Pollard, R. T., P. B. Rhines, and O. R.Y. Thompson (1973), The deepening of the wind-mixed layer, *Geophys. Fluid Dyn.*, *3*, 381–404.

Prandke, H., and A. Stips (1998), Test measurements with an operational microstructure turbulence profiler: Detection limit of dissipation rates, *Aquat. Sci.*, *60*, 191–209.

Price, J. F. (1979), On the scaling of stress-driven entrainment experiments, *J. Fluid Mech.*, *90*, 582–599.

Quadfasel, D., J.-C. Gascard, and K. P. Koltermann (1987), Large-scale oceanography in Fram Strait during the 1984 Marginal Ice-Zone Experiment, *J. Geophys. Res.*, *92*, 6719–6728.

Richman, J., and C. Garrett (1977), The transfer of energy and momentum by the wind to the surface mixed layer, *J. Phys. Oceanogr.*, *7*, 876–881.

Sakshaug, E. (2004), Primary and secondary production in the Arctic Seas, in *The Organic Carbon Cycle in the Arctic Ocean*, edited by R. Stein and R. W. MacDonald, pp. 57–81, Springer, New York.

Schauer, U., H. Loeng, B. Rudels, V. K. Ozhigin, and W. Dieck (2002), Atlantic water inflow through the Barents and Kara Seas, *Deep Sea Res., Part I*, *49*, 2281–2298.

Shay, T. J., and M. C. Gregg (1986), Convectively driven turbulent mixing in the upper ocean, *J. Phys. Oceanogr.*, *16*, 1777–1798.

Skyllingstad, E. D., C. A. Paulson, W. S. Pegau, M. G. McPhee, and T. Stanton (2003), Effects of keels on ice bottom turbulence exchange, *J. Geophys. Res.*, *108*(C12), 3372, doi:10.1029/2002JC001488.

Smith, W. O.J., and H. J. Niebauer (1993), Interactions between biological and physical processes in Arctic seas: Investigations using numerical models, *Rev. Geophys.*, *21*, 189–209.

Sundfjord, A., I. Fer, Y. Kasajima, and H. Svendsen (2007), Observations of turbulent mixing and hydrography in the marginal ice zone of the Barents Sea, *J. Geophys. Res.*, doi:10.1029/2006JC003524, in press.

Tennekes, H., and J. L. Lumley (1972), *A First Course in Turbulence*, 300 pp., MIT Press, Cambridge, Mass.

Thomson, R. E., and I. V. Fine (2003), Estimating mixed layer depth from oceanic profile data, *J. Atmos. Oceanic Technol.*, *20*, 319–329.

Thorpe, S. A., T. R. Osborn, D. M. Farmer, and S. Vagel (2003), Bubble clouds and Langmuir circulation: Observations and models, *J. Phys. Oceanogr.*, *33*, 2013–2031.

Turner, J. S. (1973), *Buoyancy Effects in Fluids*, 367 pp., Cambridge Univ. Press, New York.

Wijesekera, H., L. Padman, T. Dillon, M. Levine, and C. Paulson (1993), The application of internal-wave dissipation models to a region of strong mixing, *J. Phys. Oceanogr.*, *23*, 269–286.

I. Fer, Geophysical Institute, University of Bergen, Allégaten 70, N-5007, Bergen, Norway. (ilker.fer@gfi.uib.no)

A. Sundfjord, Norwegian Institute for Water Research, N-9296, Tromsø, Norway.